ÉCOLE POLYTECHNIQUE
FÉDÉRALE DE LAUSANNE

FACULTE ENVIRONNEMENT NATUREL, ARCHITECTURAL ET CONSTRUIT (ENAC)
INSTITUT D'INGENIERIE STRUCTURALE (IIC)
LABORATOIRE DE LA CONSTRUCTION METALLIQUE (ICOM)

Rapport EPFL N° 181194

Experimental Testing and Simulation of Bolted Beam-Column Connections having Thick Extended Endplates and Multiple Bolts per Row

Gary S. Prinz, Ph.D., P.E.
Prof. Alain Nussbaumer, Ph.D.
Shyam Khadka

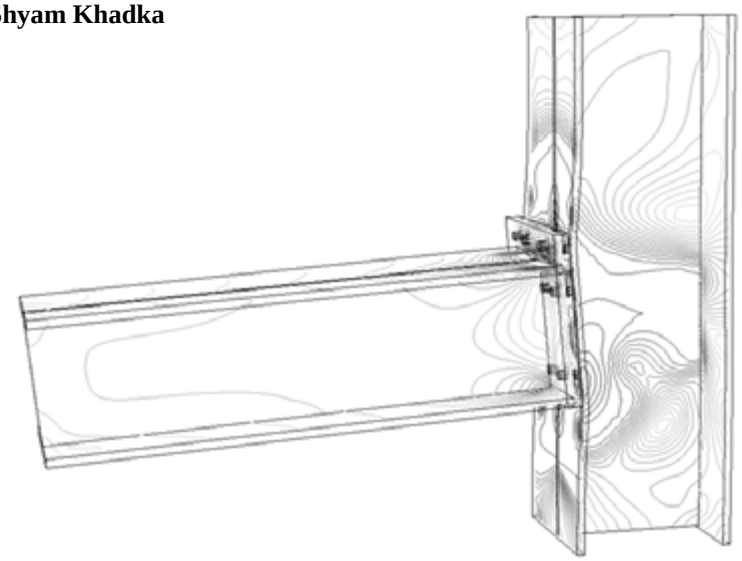

ICOM Mandat N° IC707

Final report submitted to : Centre Suisse de la Construction Métallique (SZS)

June, 2013

FACULTE ENVIRONNEMENT NATUREL, ARCHITECTURAL ET CONSTRUIT ENAC
INSTITUT D'INGENIERIE STRUCTURALE IIC
LABORATOIRE DE LA CONSTRUCTION METALLIQUE ICOM

EPFL ICOM
GC B3 505
Station 18
CH-1015 Lausanne

Téléphone : + 4121 693 24 25
Fax : + 4121 693 28 68
E-mail : icom@epfl.ch
Site web : icomwww.epfl.ch /

ÉCOLE POLYTECHNIQUE
FÉDÉRALE DE LAUSANNE

V/réf : **Lausanne, June 2013**
N/réf : GC/AN **Rapport EPFL No 181194**

Experimental Testing and Simulation of Bolted Beam-Column Connections having Thick Extended Endplates and Multiple Bolts per Row

Mandat:	SZS—Stahlbau Zentrum Schweiz Seefeldstrasse 25 CH-8034 Zurich
Définition du mandat:	Etude expérimentale avec six essais d'assemblages poutre-poteau par plaque de tête en vue de la révision de la table SZS C9 et de promouvoir les assemblages les plus économiques.
Date du mandat:	Décembre 2011 et avenant du 27 Juillet 2012
Eprouvettes:	Sept éprouvettes ont été testées. Toutes les éprouvettes ont été fabriquées par l'entreprise Sottas SA.
Réception des éprouvettes:	21 Février 2012
Dates des essais:	Mars - Juillet 2012
Chef de projet:	A. Nussbaumer
Collaborateurs:	G.S. Prinz, S. Khadka, G. Rouge, S. Demierre, P. Maurice, F. Dubugnon
Auteurs du rapport:	G.S. Prinz, A. Nussbaumer, S. Khadka
Directeur de l'ICOM:	J.-P. Lebet

Signatures :

Chef de Projet

Prof. Dr. Alain Nussbaumer

Directeur de l'ICOM

Prof. Dr. Jean-Paul Lebet

Ce rapport contient 34 pages

Acknowledgements

This report presents the results of a research project sponsored by the Swiss Institute of Steel Construction (SZS). We acknowledge the financial support provided by SZS and by Sottas SA, who fabricated the test specimens. The assistance and encouragement of the SZS technical committee is also appreciated. The research was conducted in the Steel Structures Laboratory (ICOM) at the Ecole Polytechnique Federale de Lausanne (EPFL). Laboratory staff instrumental in the completion of this work include: Sylvain Demierre, Gerald Rouge, and Frederique Dubugnon. Many thanks also go to Luis Borges for his help with the Eurocode 3, part 1-8, component method analyses, Mr. Paul Maurice for his assistance with the test specimen preparation, and to Christoph Gemperle for his guidance as a member of the new Table C-9 working group. Although many individuals contributed to the research findings presented herein, the authors accept full responsibility for the conclusions presented.

Project Publications

The following list represents the scientific publications resulting/pending from the experimental study.

1. Prinz, G.S., Nussbaumer, A., Borges, L., and Khadka, S. “Experimental testing and simulation of bolted beam-column connections having thick extended endplates and multiple bolts per row.” *Engineering Structures* [under review].

Table of Contents

List of Figures

List of Tables

Report Abstract

Retrofit of existing steel buildings often requires strengthening of the connection regions. One common connection, the bolted beam-column connection, is often strengthened in design using stiffened extended endplates, or with column web stiffeners welded between the column flanges. In a retrofit scenario, adding stiffeners to the endplate is difficult due to the concrete slab and metal deck, and excessive field welding of column web stiffeners may be uneconomical. Simplifying retrofit efforts, and for economy, connection strength may be improved by simply adding additional bolts to the connection. Current code methods, broadly generalized to all connection configurations, are based on component experiments having only two bolts per row (one bolt on either side of the column web). This study experimentally investigates strengthening of bolted beam-column connections using more than one bolt on either side of the column web. Six full-scale bolted beam-column connections are tested, representing exterior beam-column connections (beams attached to only one column flange). Connections with both extended and flush endplates are considered. Two column sections (HE300A and HE300B) are tested along with HE300B beams creating both equal-column/beam, and weak-column strong-beam scenarios. Analytical simulations provide insight into local connection demands, and experimental results are compared with current code methods. The experiments indicate that using multiple bolts per row increases connection moment capacity but decreases rotation capacity (connection ductility) due to increased bolt prying forces from column flange distortions. With the exception of specimen T-3B which failed through bolt-thread shear after 0.02rad, all connections with multiple bolts per row still achieved rotations greater than 0.06rad. The NASCON software, which is based on Eurocode 3 component method, conservatively predicted the connection strength of each test specimen, including weak-column strong-beam assemblies, and accurately identified the initial connection limit state.

1. Introduction

Understanding the strength and rigidity of connection regions is necessary for the efficient design of steel building systems. One common steel building connection, the bolted beam-column connection, is often assumed in design as either fully pinned or fully rigid; however in reality, the rigidity of such connections is generally somewhere in-between (a semi-rigid connection). The required strength of beams and columns depends directly on considerations made for the connection rigidity [1]. Moreover, in retrofit scenarios where strengthening of connections is needed, accurate understanding of existing and improved strength and rigidity is required. To estimate the true strength and rigidity characteristics of bolted beam-column connections, the EuroCode has adopted the component method [2] which considers individual connection components (bolts, flanges, webs, endplates, etc.) and their interactions.

The component method presented in the EuroCode 3, part 1-8 (hereafter referred to as EC3-1.8) is based on research published in the early 1980's by Zoetemeijer [3,4] and can be summarized in five general steps: 1) identification of the load-path through the connection; 2) determination of individual component strength within the load path (for example, the compressive strength of the column web, tensile strength of the beam flange, etc.); 3) determination of individual component stiffness in the load path; 4) assembly of the individual components in series and or parallel (depending on their arrangement); and 5) determination of the "weakest link" in the load path based on strength and deformation capacity. Figure 1 shows a typical beam-column connection and the component method representation. Figure 2 presents a detailed flowchart of the component method analysis procedure including reference to code sections.

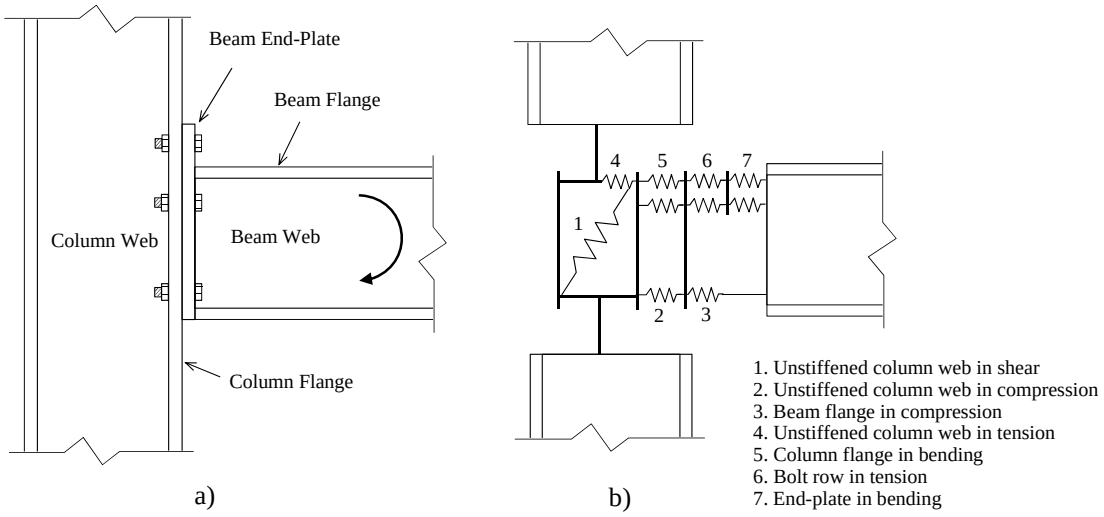

Figure 1. a) Typical beam-column bolted connection and b) component method representation.

Many analytical and experimental studies have investigated bolted beam column connections [5,6,7,8,9,10,11,12] along with the predictive capabilities of the EC3-1-8 component method. One such study by Abidelah et al. [13] investigated the strengthening of bolted beam-column connections by comparing configurations with and without stiffeners in the extended endplate portion. In [13], results showed that additional endplate stiffeners increase moment capacity but decrease connection ductility. The EC3-1.8 component method accurately predicted the connection failure modes in the strengthened connections; however, connection strength was consistently under-predicted. All connections in [13] had two bolts per row and column web stiffeners were not used.

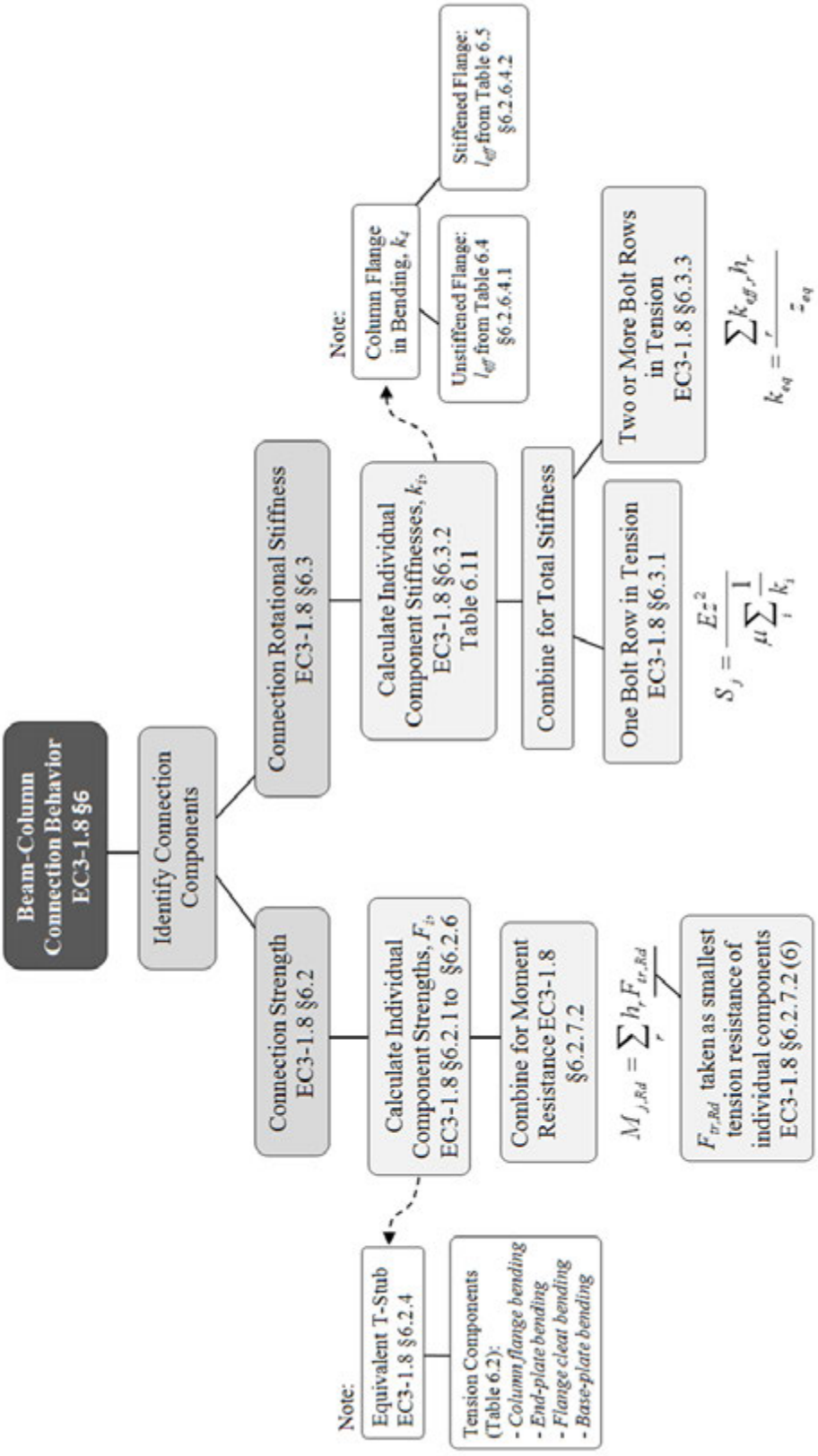

Figure 2. EC3-1.8 component method flow chart.

Although connection strength may be increased using endplate stiffeners, in a retrofit scenario adding endplate stiffeners is difficult when a concrete slab or metal deck is present. Adding another bolt on either side of the column web (compare bolt configurations in Figure 3) may result in similar connection strength gain while simplifying retrofit application. Additionally, it is often more economical to use multiple bolts per row when wide H-sections are used [14]; however, current code methods, broadly generalized to all connection configurations, are currently based on T-stub experiments [3,4] having only one bolt on either side of the column or beam web.

Limited experimental data is available for comparing the performance of the EC3-1.8 component method with connection configurations having multiple bolts per row. The authors are aware of a finished European study with beam-column experiments having multiple bolts per row performed by the research group of Professor Ungermann at TU Dortmund (through personal communication); however, the results of such experiments are not available and have not yet been published in the literature. Additionally, Demonceau et al. [14] claim that many tests on beam-column connections having multiple bolts per row were carried out, but the data are “no more available nowadays”.

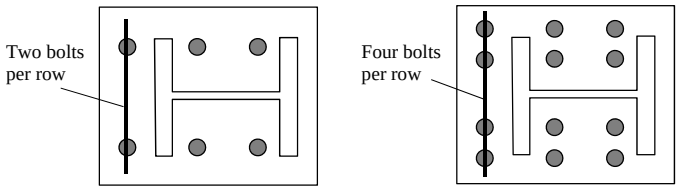

Figure 3. a) Connection with two bolts per row and b) connection with four bolts per row.

This study experimentally investigates the interactive behavior of bolted beam-column connections having thick extended endplates and four bolts per row (without column web stiffeners). Weak column strong beam situations are considered. Six beam-column connections having various bolt configurations and section dimensions are tested up to failure to determine connection performance. Detailed numerical models are also created to determine stress and strain distributions within the connection regions, and to investigate the feasibility of simulating semi-rigid bolted connections having four bolts per row. Both the experimental and analytical tests are compared with the current EC3-1.8 component method. The study begins with an overview of the experimental program, followed by the numerical modeling methods and result comparisons. Conclusions on the performance of bolted beam-column connections with thick extended end-plates and four bolts per row are provided.

2. Experimental Program

An experimental program was developed to determine the static monotonic behavior of bolted beam-column connections having multiple bolt configurations, with the main objectives being: 1) determine the influence of bolt grouping (multiple bolts per row) and thick endplates on connection response; 2) determine the different connection failure modes; and 3) compare experimental performance with code methods. The following sections discuss the experimental program in detail and present results based on the objectives outlined above.

2.1. Test Specimens

The experimental specimens consist of a column element and a beam element fully welded to an endplate. The beam and column elements are connected using multiple GR 10.9 M20 bolts with GR10.9-HV nuts and standard GR4.6 washers. All bolts are pre-tensioned to 480 N-m as per [15]. A total of six beam-column connections are considered, representing three different bolt configurations (both extended and non-extended configurations) and two column profiles. All beam and column elements are fabricated from S235 steel while the endplates are fabricated from S355 steel following typical practice. Figure 4 shows the specimen geometry including endplate and bolt group details; Table 1 shows the experimental test matrix; and Table 2 presents the specimen material properties, as provided by the steel fabricator. Shown in Table 1, the column profile tested in group A (specimens 1A, 2A, and 3A) is an HE 300A section having a web thickness of 8.5mm and a flange thickness of 14mm; the column profile tested in group B is an HE 300B section having a larger web and flange thickness (11mm and 19mm respectively). The beam (HE 300B) is the same for all specimens, creating a weak-column strong-beam scenario for specimens 1A, 2A, and 3A. The endplate thickness of each specimen is 30mm.

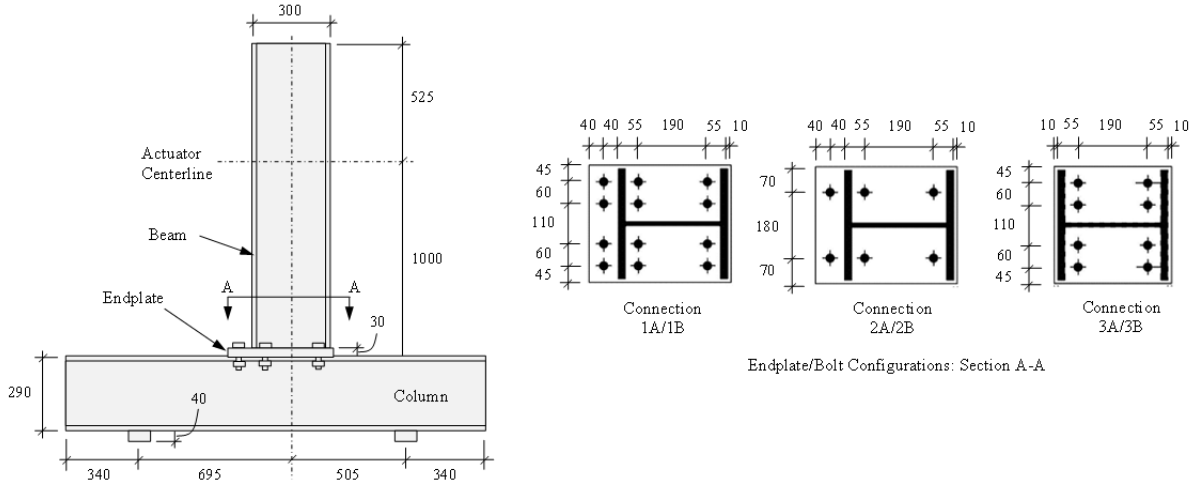

Figure 4. Test specimen geometry.

Table 1: Test Matrix

Specimen	Column Element	Beam Element	Number of Bolts	Bolt/ Endplate Configuration
1A	HE 300A	HE 300B	12	
2A	HE 300A	HE 300B	6	
3A	HE 300A	HE 300B	8	
1B*	HE 300B	HE 300B	12	
2B	HE 300B	HE 300B	6	
3B	HE 300B	HE 300B	8	

* Note two 1B specimens were tested due to an experimental error (discussed later in the Experimental Results section)

Table 2: Beam, Column, and Endplate Material Characteristics

Material Grade	Element	Yield stress [MPa]	Ultimate Stress [MPa]	Fracture Strain [ε_f]	Chemical Composition										
					%C	%Mn	%P	%S	%Si	%N	%Cu	%Ni	%Cr	%V	%Mo
S235 JR+M	HE 300A	353	433	0.320	0.060	0.670	0.033	0.026	0.220	0.009	0.390	0.160	0.160	0.007	0.040
S235 JR+M	HE 300B	346	433	0.320	0.070	0.660	0.030	0.026	0.180	0.009	0.360	0.190	0.200	0.006	0.030
S355 J2+N	Endplate	366	538	0.279	0.190	1.470	0.015	0.009	0.220	0.006	0.060	0.030	0.030	0.002	0.005

2.2. Test Configuration, Instrumentation, and Loading

The experimental setup shown in Figure 5 is designed to investigate the response of bolted beam-column connections during beam overloading. In Figure 5, the column section rests horizontally on two supports, preventing column-flange contact with the ground and allowing column rotations within the connection region; the beam extends vertically from the column, and is connected to a horizontal actuator where the displacement controlled loading is applied. To prevent sliding of the specimen during loading, four pre-tensioned rods (two on either side of the column web) clamp the column flange to the testing floor.

Various measuring devices attached to the specimen are used to record local and global connection behavior. Twelve unidirectional strain gauges and four linear variable differential transducers (LVDTs) are attached to each specimen to record local member strains and global connection displacements. Two strain gauges located on each beam flange near the connection (four gauges in total) allow for determination of beam moment demands; four strain gauges located on each side of the column web near the connection (eight gauges in total) measure local column web demands; two LVDTs located on the extended portion of end-plate (on the column flange for the flush endplate connections) determine plate uplift; one LVDT attached to the column element records any slip between the column and floor; and a single horizontal LVDT attached to the beam at the centerline of the horizontal actuator records beam displacements. Figure 5 shows the applied instrumentation. With the instrumentation setup in Figure 5, connection rotations in this study are calculated as $\theta = (\text{LVDT}_1\text{-LVDT}_2)/L$.

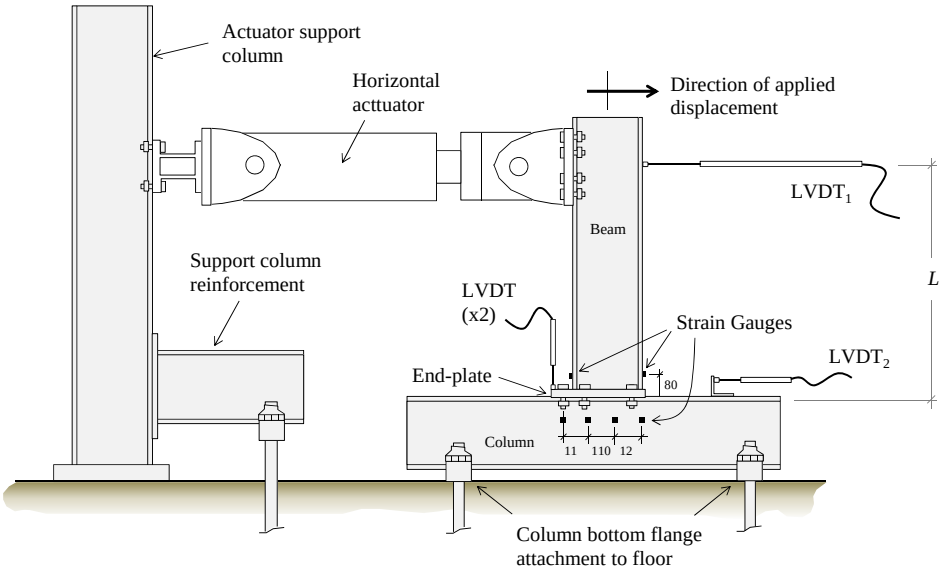

Figure 5. Experimental setup with instrumentation locations.

The connection loading protocol consists of two phases: 1) elastic load and unload to engage specimen supports and bolt threads, and 2) static monotonic loading up to connection failure. In the first loading phase, 3mm of displacement is applied and then removed at a strain rate of 0.1mm/sec. Following, monotonic loading up to failure is applied at a strain rate of 0.1mm/sec for the remainder of the test. Ultimate failure is defined in this study as a 20% reduction in moment capacity.

3. Experimental Results

3.1. Observations and Governing Failure Modes

Two failure limit levels are considered, 1) a classical failure limit based on initial component yielding (used to compare code methods and experimental results), and 2) an ultimate failure limit defined as a 20% reduction in connection moment capacity. In each test, column flange capacity was observed to be the initial limiting component, with large deformations clearly visible within the connection tensile zone (similar to Figure 6). Residual flange deformations after testing indicated significant yielding. Following large flange deformations, bolt failure occurred in each test, reducing connection capacity to below 80% of ultimate.

For beam-column connections having extended endplates, complete bolt fracture always occurred in the extended section on the bolt group closest to the column web; for beam column connections with flush endplates, bolt failure occurred in the tensile zone on the bolt group closest to the column web. Higher demands on the bolts nearest the column web are attributed to relative deformations between the endplate and column flange created from the increased flange stiffness near the web (see Figure 6). As column flange deformations increase, flange behavior transitions from flexural to membrane action, increasing bolt prying demands making bolt failure unavoidable. Figure 7 shows this flexural-to-membrane flange transition, which occurs near 0.04rad of rotation for the geometries tested in this study.

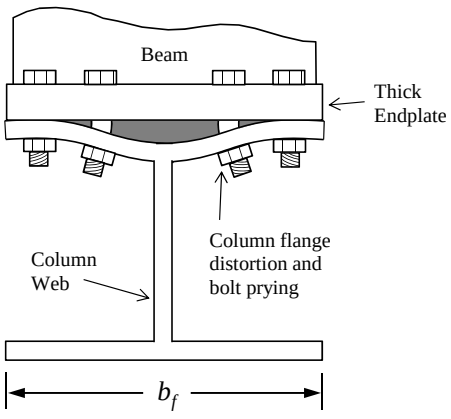

Figure 6. Column flange distortion and bolt prying

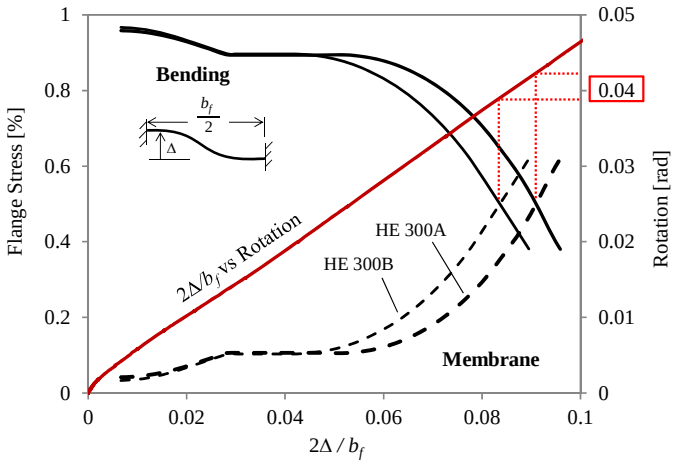

Figure 7. Flange flexural-to-membrane behavior transition and corresponding connection rotation (note b_f is the total flange width and Δ is the flange distortion).

Excepting specimen T3B (having a flush endplate), tensile fracture of the complete bolt cross-section occurred in each test after the 0.04rad flexural-to-membrane flange transition limit. In specimen T3B, bolt-thread shear failure occurred at 0.027rad of rotation. Figure 8 shows the fractured bolts for specimens T1A through T3A and bolt-thread shear for specimen T3B.

Following bolt fracture, permanent deformation was observed in the GR4.6 washers (bending and compressive yielding, see Figure 9). The influence of washer deformations on bolt demands and connection performance are not known. The performance of the GR4.6 washers compared to standard high-strength washers was identical, as will be explored with T-stub tests later in Section 4.

Figure 8. Beam-column connection bolt failures.

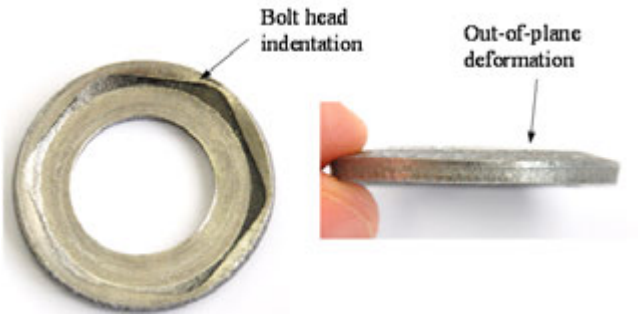

Figure 9. Deformed washer from critical bolt in specimen T3A.

The testing conditions of specimens T1A and T1B (the first two specimens tested) differed slightly from the remaining four tests due to unanticipated issues with the test setup and instrumentation. The following sections (3.1.1 and 3.1.2) describe the test T1A and T1B observations to clarify these differences.

3.1.1. SpecimenT1A

Figure 10 shows the moment rotation curve for test specimen T1A. Note in Figure 10 that the specimen was unloaded after 0.02rad due to excessive movement of the actuator support column. Following reinforcement of the actuator support column, the specimen was reloaded up to nearly 0.05rad where lateral movement of the beam began (lateral buckling due to column web instability). Prior to this lateral beam movement, the peak applied moment was 224 kN-m, and significant deformation of the column flange near the extended end-plate was noticed. In realistic beam configurations, this lateral beam movement is restrained by transverse girders and the presence of a concrete slab; therefore, beam guide rails were added and the specimen was reloaded up to failure. The observed failure mode was bolt fracture in the extended plate section closest to the column web (see Figure 10), due to excessive deformations and prying between the endplate and column flange.

Figure 11 shows local deformation of the column flange at the edge of the end-plate. Figure 12 shows the connection rotation during testing with large deformations of the column flange and web.

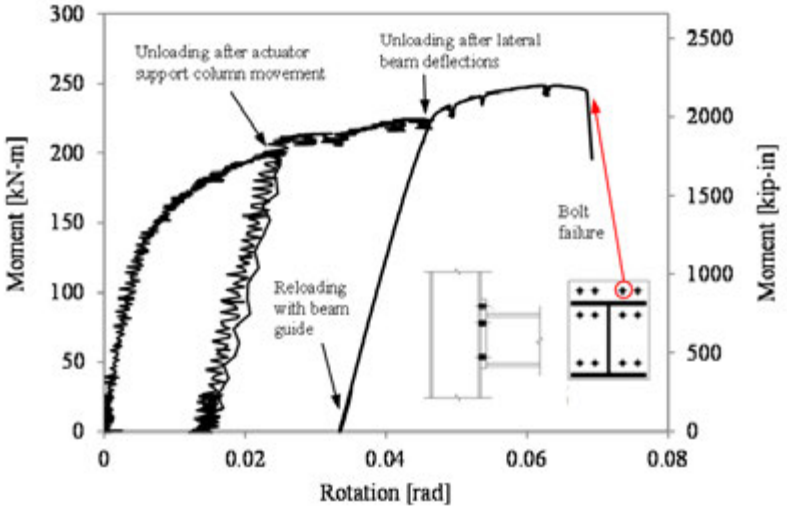

Figure 10. Moment-rotation curve for specimen T1A.

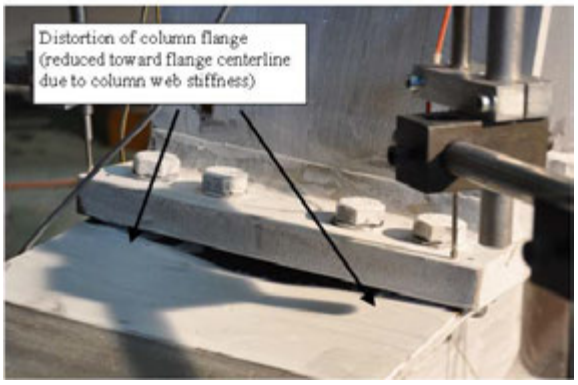

Figure 11. Column flange deformation.

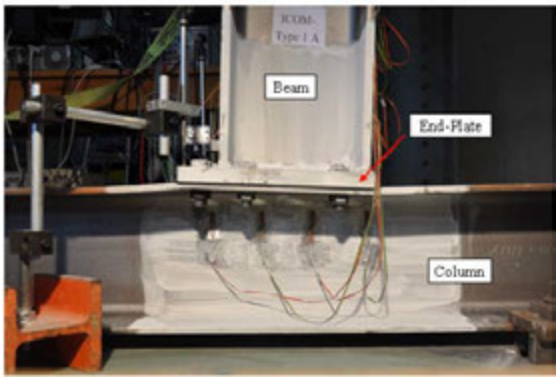

Figure 12. Connection rotation at peak applied moment.

3.1.2. SpecimenT1B

Specimen T1B was tested prior to the installation of the horizontal LVDT accounting for slip, and slip occurred. During testing, relaxation of the pre-stressed rods clamping the column flange to the floor allowed the beam-column assembly to translate (slip), affecting rotation measurements. Figure 13 shows the resulting moment rotation curve for specimen T1B which is elongated on the rotation axis due to the slip. In Figure 13, the provided moment values are unaffected by the slip.

The resulting failure mode for specimen T1B was bolt fracture in the extended endplate section closest to the column web. Excessive deformations between the beam endplate and column flange were noticed. The column web prevented local flange deformations leading to prying between the thick endplate and inner bolt group (the bolt group nearest the column web). Figure 14 shows the deformed shape of the beam-column assembly corresponding to the peak moment (just after bolt failure).

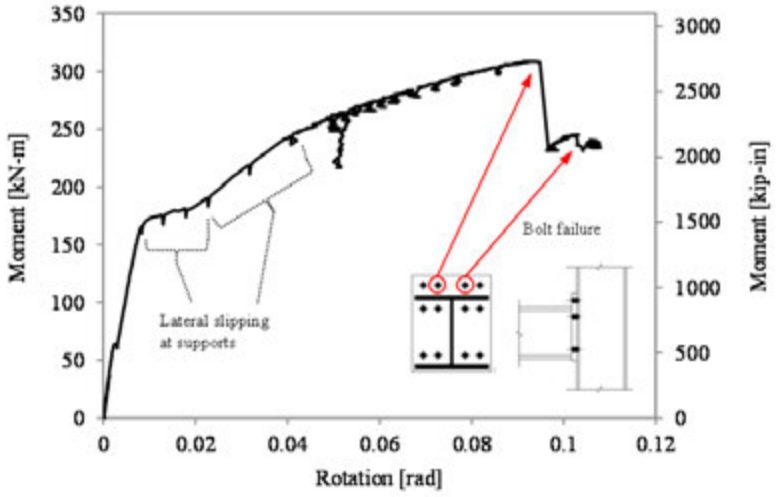

Figure 13. Moment-rotation curve for specimen T1B.

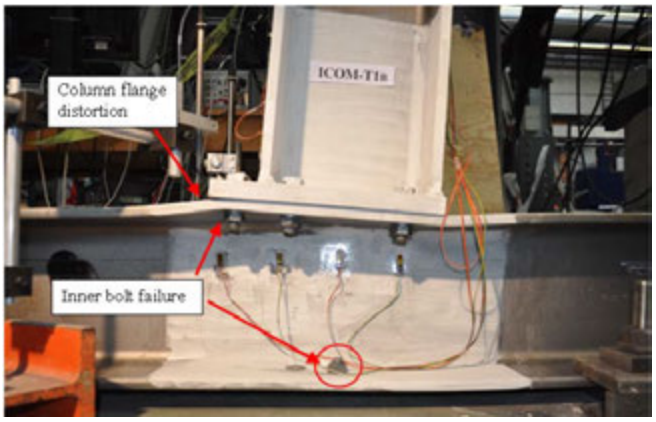

Figure 14. Connection rotation at peak applied moment.

3.1.3. Specimen T1B(2)

Due to the translational slip of specimen T1B which prevented accurate determination of connection rotation, an additional TIB specimen was prepared and tested [named T1B(2)]. Similar to specimen T1B, the resulting failure mode for specimen T1B(2) was bolt fracture in the extended endplate section closest to the column web. With specimen T1B(2), simultaneous fracture of both bolts in the extended endplate (nearest the column web) occurred. Again, deformations between the beam endplate and column flange were noticed prior to bolt fracture. Connection rotation behavior for specimen T1B(2) will be discussed in the following section on Moment-Rotation Behavior.

3.2. Moment-Rotation Behavior

The use of four bolts per row and extended endplates increases connection moment capacity but may reduce rotation capacity. Figure 15 shows the moment rotation behavior for all six beam-column connection configurations. As could be expected, extended endplate configurations having four bolts per row (specimens T1A and T1B, T1B(2)) achieved higher moment capacity than the corresponding specimens having two bolts per row (specimens T2A and T2B) (on average 29.5% higher capacity).

Weak-column strong-beam extended endplate specimens with only two bolts per row achieved 52% more rotation than corresponding specimens with four bolts per row (compare T1A and T2A). This increase in rotation capacity is likely due to the flexible column flange and increased distance between the bolt and column-web, resulting in decreased rotational stiffness and decreased prying between the endplate and column flange at comparable rotation values (see again Figure 6). A similar increase in rotation capacity was not observed between the equal column-beam specimens having thicker column flanges (compare specimens T1B(2) and T2B). Table 3 shows the strength, stiffness, and ultimate rotation values for each test. Note in Table 3 that the rotational stiffness of specimen T1A, having four bolts per row, is more than twice that of specimen T2A having two bolts per row.

All specimens having extended endplates achieved higher moment resistance than the flush endplate connections. Comparing specimen T2A (having an extended endplate and two bolts per row in the connection) with specimen T3A (having a flush endplate and four bolts per row) indicates 34% higher capacity with the extended endplate connection (see Figure 15).

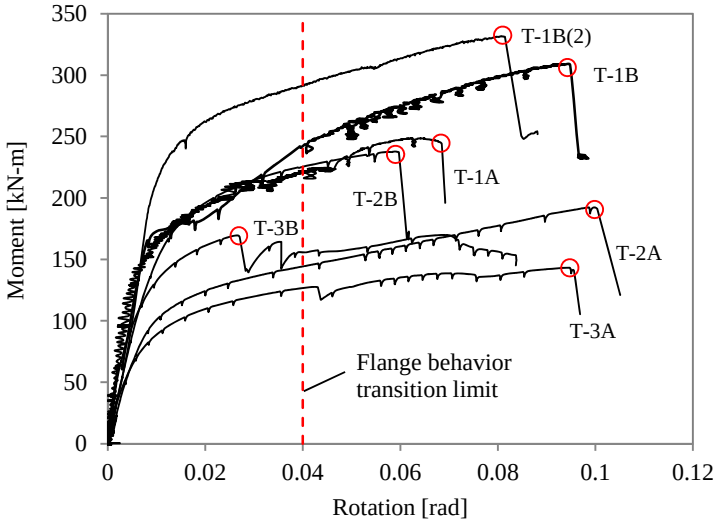

Figure 15. Moment-rotation behavior for all six test specimens.

Table 3: Connection strength, elastic stiffness, and rotation values.

Specimen	No. of Bolts	Ultimate Strength [kN-m]	Rotational Stiffness [kN-m]	Peak Rotation [rad]
T1A	12	248.6	26341	0.069
T2A	6	192.4	12346	0.105
T3A	8	143.2	14268	0.097
T1B	12	308.7	21153	0.098*
T1B(2)	12	331.7	22313	0.081
T2B	6	237.8	17577	0.062
T3B	8	169.9	27277	0.027**

* Specimen experienced lateral slip during testing

** Reduction to 80% of ultimate capacity after 0.027rad, specimen regained strength and achieved 0.084rad

3.3. Effect of Column Section and Bolt Group on Web Strains

Figure 16 shows the distribution of column-web strains for each connection configuration. The column-web strains in Figure 16 represent only transverse web compression and tension as flexural strains (induced through web bending) were removed by averaging of the strain gauge readings. As could be expected, extended endplate connections having four bolts per row experienced higher column web strains than the corresponding connections having two bolts per row (300% higher for column sections HE300A, and 66% higher for column sections HE300B). This increase is likely due to the closer spacing of the bolts, relative to the column web, created from the additional bolts. Additionally, with the exception of specimen T3B which experienced early bolt-thread shear failure, specimens having HE300B column sections (specimens in Group B, see Figure 16) experienced higher column web strains. This is likely due to increased resistance of the column flange transferring higher connection demands to the web. The strain required to initiate web material yielding was exceeded in each test. Interestingly, the neutral axis remained relatively constant between connection configurations.

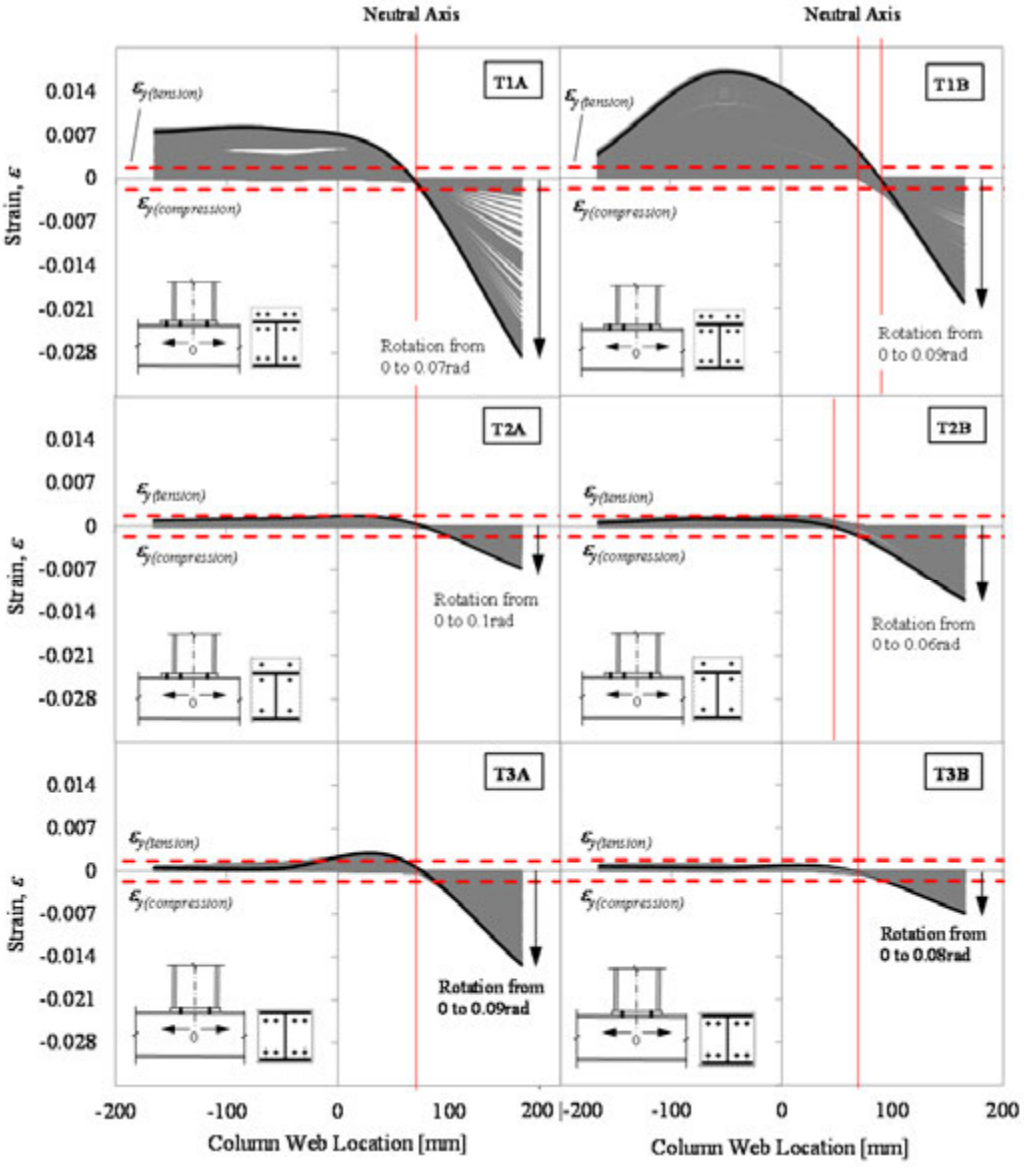

Figure 16. Column-web strain distribution.

4. Effect of GR4.6 Washers on Bolt Load and Pre-Stress

To explore the influence of washer strength on bolt demands, including effects on bolt pre-stressing, two T-stub connections are fabricated using two GR10.9 HV bolts. The bolts are constructed with both GR4.6 and GR10.9 washers. The T-stub connections are fabricated from an HE300B section cut in half at the web centerline, and tested in a universal testing machine with a 1000kN capacity. Similar to the beam-column experiments, all bolts are pre-tightened to 480N-m as per [15] using a pre-set torque wrench. Figure 17(a) shows the specimen setup including T-stub geometry and bolt locations.

Each bolt is instrumented with two unidirectional strain gauges positioned 180 degrees apart and fixed near the bolt surface (see Figure 17(b)). Attaching gauges on opposite sides of the bolt surface allows for determination of prying strains during expected deformations of the T-stub.

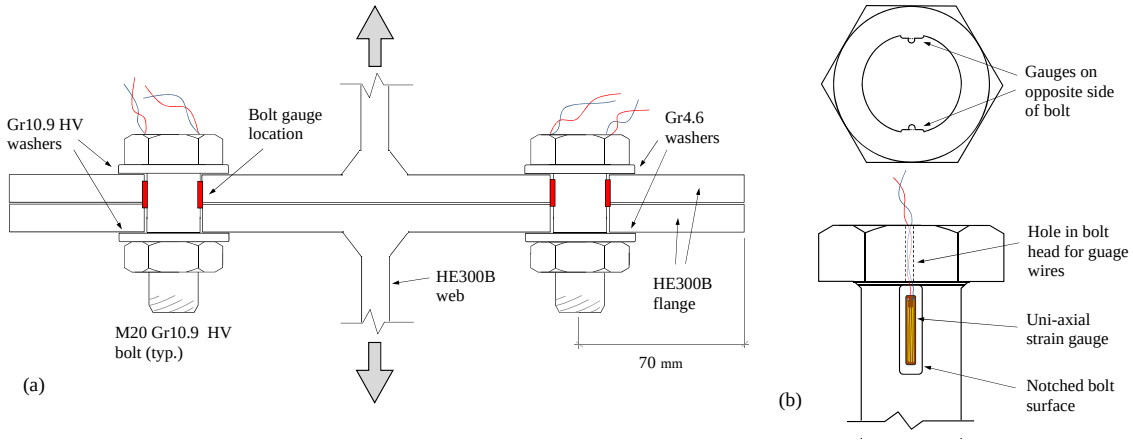

Figure 17. (a) T-stub specimen geometry and bolt locations (b) bolt instrumentation.

Results indicate that the use of GR 4.6 washers, rather than GR 10.9 HV washers, has negligible effect on the applied bolt pre-stress. Figure 18 shows the measured axial pre-stress between the bolts having GR 4.6 and GR 10.9 HV washers, with less than 15MPa difference after the applied torque. This indicates similar friction resistance for both washer strengths, and suggests accurate application of bolt pre-stress in the beam-column tests.

Measured prying strains between the two bolts were similar, but slightly larger for the GR 10.9 HV bolt. During testing of the T-stub connection, failure of the GR 10.9 HV bolt governed the connection capacity. Figure 19(a) shows the distribution of strains in each bolt at the peak applied load, and Figure 19(b) shows the evolution of bolt surface strains during loading. From Figure 19(a), similar strain distributions are observed between the two bolts, with a 26% higher maximum tensile strain value for the GR 10.9 HV bolt. In Figure 19(b), this significant bolt prying occurs near an applied load of 300kN; however, as evident in Figure 19(b), bolt bending is also induced from the applied pre-tensioning.

Similar pre-stress values and prying strains between the two bolts suggests that the GR 4.6 washers had a negligible effect on the experimental values obtained for the beam-column specimens.

Calculations using the EC3-1.8 T-stub capacity equations suggest flange yielding as the governing T-stub failure mode. From the EC3-1.8 calculations, the flange yielding capacity (mode 1 failure) is calculated as 169kN whereas capacities for mode 2 (flange-yielding with bolt fracture, including prying) and mode 3 (bolt tensile fracture) are 228kN

and 352kN respectively. Comparing calculated capacities with the T-stub response in Figure 19(b), the predicted limit state of flange yielding is overly conservative; however, the EC3-1.8 method appears to predict the mode 2 failure limit (bolt fracture with flange yielding) with reasonably accuracy.

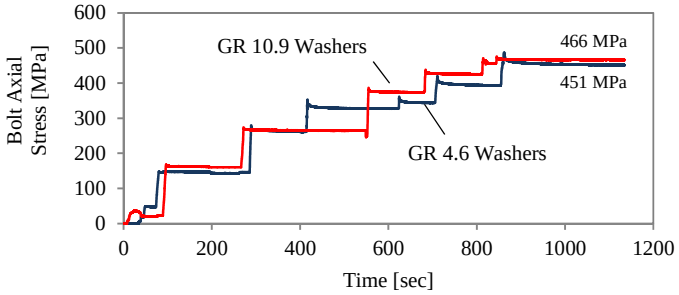

Figure 18. Measured bolt axial pre-stress.

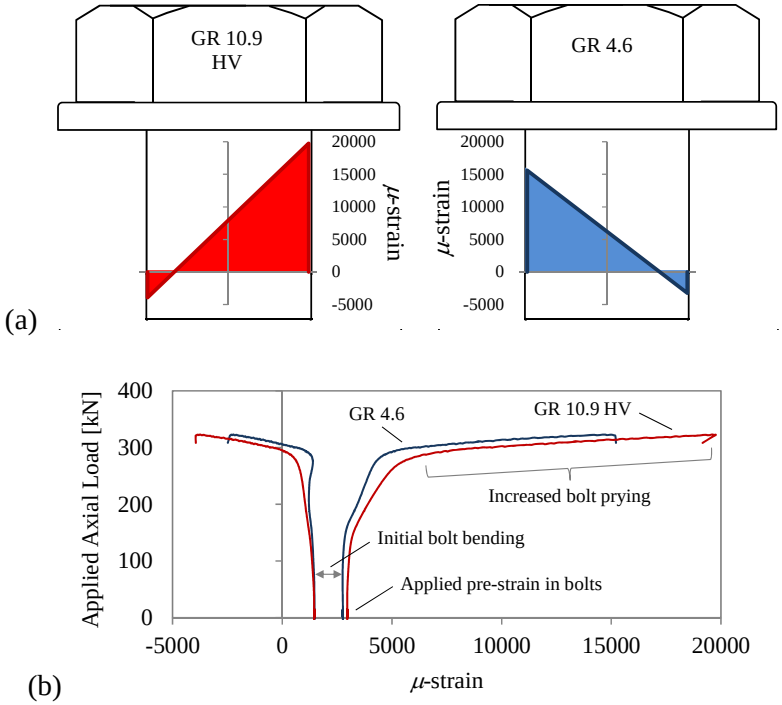

Figure 19. (a) Peak measured surface strains and (b) evolution of bolt surface strains during loading.

5. Numerical Modeling

To investigate parameters not measured experimentally, such as bolt forces and continuous connection stresses, each test configuration is analyzed using finite elements. All finite element models are validated using the experimental data. The following sections present the connection modeling techniques, including: element selection, mesh refinement, bolted interaction, boundary conditions, and material properties. Results from the simulations and validation will be presented later in the Numerical Results section.

In addition to finite element modeling and for comparison, the behavior of each connection is also predicted using the EC3-1.8 component method. Comparison and results are presented later in the Numerical Results section.

5.1. Finite Element Modeling Methods

Three-dimensional finite elements, nonlinear multi-directional springs, and various boundary conditions are used to simulate the connection test setup. To allow for detailed determination of stress and strain states throughout the connection assembly, shell elements model the beam web, beam flanges, end-plate, column web, and column flanges. All shell elements are located at the member section centerlines. Pinned boundary conditions at the column ends simulate the column-to-floor attachment in the test, and an applied displacement at the beam tip simulates the horizontal actuator. To prevent local stress concentrations at the pinned column ends and beam tip, rigid nodal constraints distribute the effects throughout the entire member cross-section. Figure 20(a) shows the model boundary conditions and applied constraints. The welded connection between the beam and end-plate is assumed fixed. The bolted interaction between the end-plate and column is simulated using nonlinear multi-directional springs, where the axial and shear resistance of the bolt are input as nominal values. To prevent local stress concentrations at the shell-spring junction, the spring force is distributed over a shell area equal to the area of the bolt diameter using rigid nodal constraints (see Figure 20(b)). All analyses are performed in ABAQUS [17] and consider nonlinear geometry (large displacement) effects.

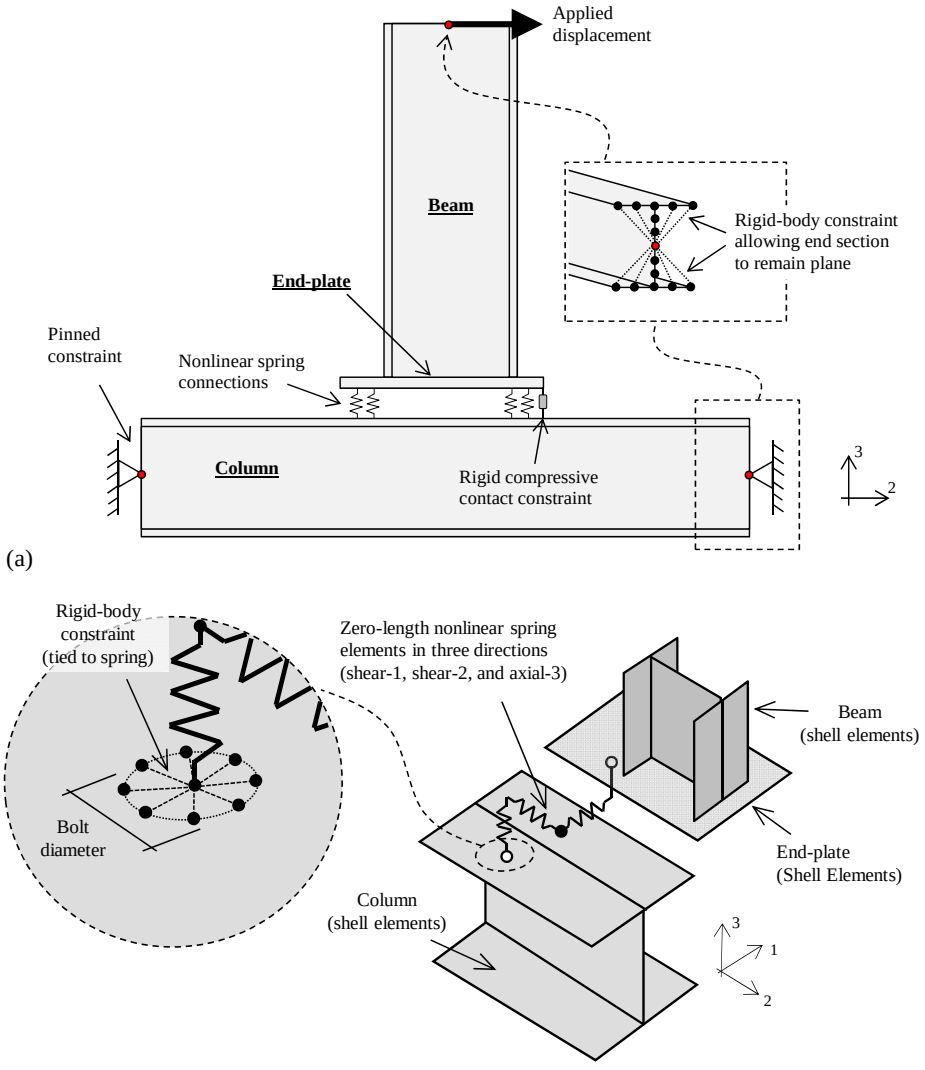

Figure 20. (a) Boundary conditions for beam-column connection and (b) modeling techniques for column-to-endplate bolted connection.

5.1.1. Material Properties

Steel material behavior in the beam, column, and end-plate is simulated using a bi-linear material hardening model. Material properties (yield strength, ultimate strength) for the hardening model were taken from the material data provided in Table 2.

Constitutive properties for simulating bolt resistance are based on tested strength-deformation values for M20 10.9 bolts, obtained by other researchers [11]. A multi-linear material model simulates bolt behavior while in tension, and because the beam endplate is in contact with the column flange while in compression, the bolt is given infinite compressive stiffness. Figure 21 shows the multi-linear bolt behavior in terms of the bolt yield stress. The bolt yield stress, F_y, used in this study is 990MPa.

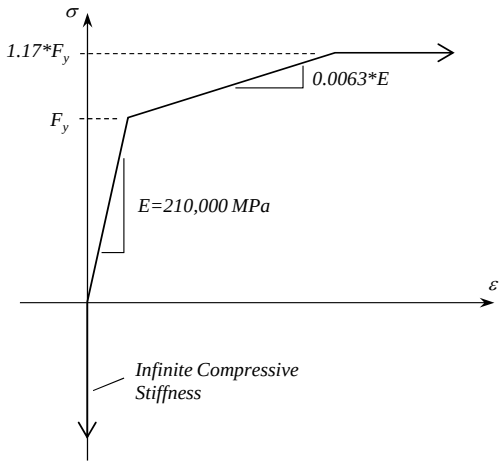

Figure 21. Bolt material behavior

5.2. Component methods

The EC3-1.8 component method can be used to predict the onset of yielding. This method served as a basis to a numerical analysis tool called NASCON [18,19]. This software does the computations according to the EC3 method. It also contains an extension which allows the prediction after yielding onset and thus post-limit stiffness and ductility of the joints.

For each connection configuration, NASCON is used to apply both strictly the EC3-1.8 method (called in the results chapter EC component method), as well as the prediction after yielding (called NASCON method). For the NASCON method, computations are made using the component material data provided in Table 2, nominal member dimensions provided in [16], and bolt behavior as described above for the finite element modeling. For the EC3-1.8 component method, computations are made using Swiss code guaranteed material values as well as resistance factors, i.e. the values computed correspond to application of the code in engineering offices.

6. Numerical Results

6.1. Comparison between FEA, Experimental Response, and Component Methods

The finite element simulations are able to capture the global inelastic moment-rotation behavior observed in the experimental tests, while the NASCON method significantly under-predicts the observed moment resistance. Figure 23 shows the moment-rotation

comparison between the finite element analysis, experimental measurements, and the NASCON method. Table 4 presents the rotational stiffness, peak rotation (rotation at peak applied load), comparative strength values at 0.02rad, and the different failure limits for the experiments, analyses, the NASCON as well as the EC3-1.8 component method. One can notice that, logically, the EC3-1.8 component method values are systematically lower than the NASCON values.

The value 0.02 rad was chosen due to the early failure of specimen T3B; and is still over two times the theoretical rotation required to achieve the fully plastic (P-P) state for an HEB300 beam of 9m (assuming rigid fixation to the column, see Figure 22). Note that the classical failure limit predicted by the ABAQUS and NASCON simulations is based on the location of initial yielding. At a rotation of 0.02rad, all finite element simulations are within 12% on average of experimental observation. For specimen T3B, the model values are above the experimental ones. But overall, the finite element simulations fit reasonably with the experiments. Note that experimental values for T1B are lower than the model values due to the specimen slip, but match well with T1B(2) having no slip.

The NASCON method usually leads to lower values than the finite element simulations, except for T2A. The EC3-1.8 component method values are always on the safe side by at least 11% (note that with the EC3-1.8 method resistance factors are included). For test specimens T1A, T2A, and T3A having smaller column cross-sections, the initial connection stiffness is slightly under-predicted by the finite element simulations (see Figure 23, and the values presented in Table 4); the stiffness predicted both by the NASCON and the EC3-1.8 component methods are close to experimental results. To conclude, one can say that the use of multiple bolts per row increases connection moment capacity but decreases rotation capacity (connection ductility) due to increased bolt prying forces and earlier bolt failure from column flange distortions (compare experimental result for specimen T1A and T2A in Figure 23).

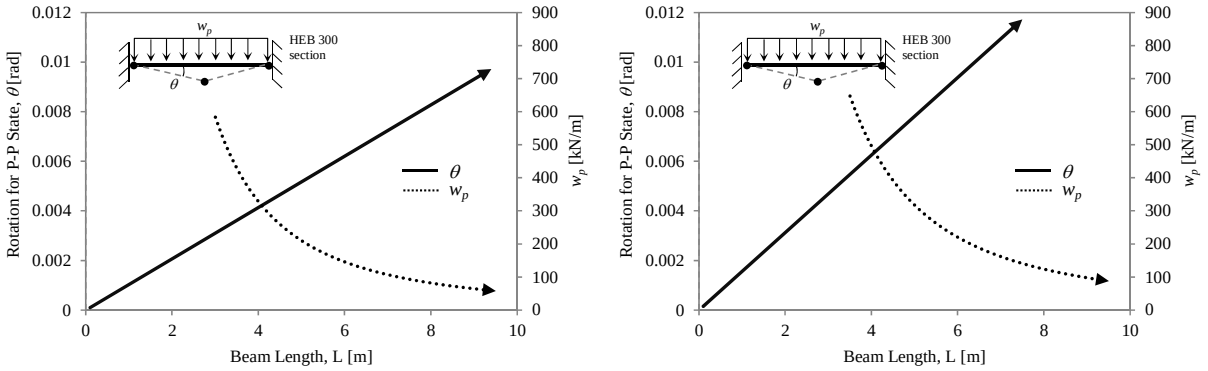

Figure 22. Beam rotation and applied load required to achieve P-P state versus beam length; for HEB 300 sections of (a) S235 material and (b) S355 material.

In addition to the global connection behavior, eight strain gauges located on both sides of the column webs allow for validation of the finite element techniques through comparison of localized member strains (vertical column web strains). Local member strains cannot be determined using the component methods. Strain values from the finite element models were taken at the same geometric location as the applied strain gauges in the experimental tests. Figure 24 shows the distribution of column web strains for each test (values taken near the peak connection rotation) and the corresponding prediction from the

finite element simulation. From Figure 24, the connection simulations adequately capture the local member behavior, with configuration T3A being within 8% of the experimental readings and the largest discrepancy being 43% in the column web compression zone of configuration T1A.

With confidence in the global and local model behavior, the finite element simulations can be used to investigate parameters not easily obtained during experimental testing (localized bolt demands, connection stress distributions around bolt holes, etc.).

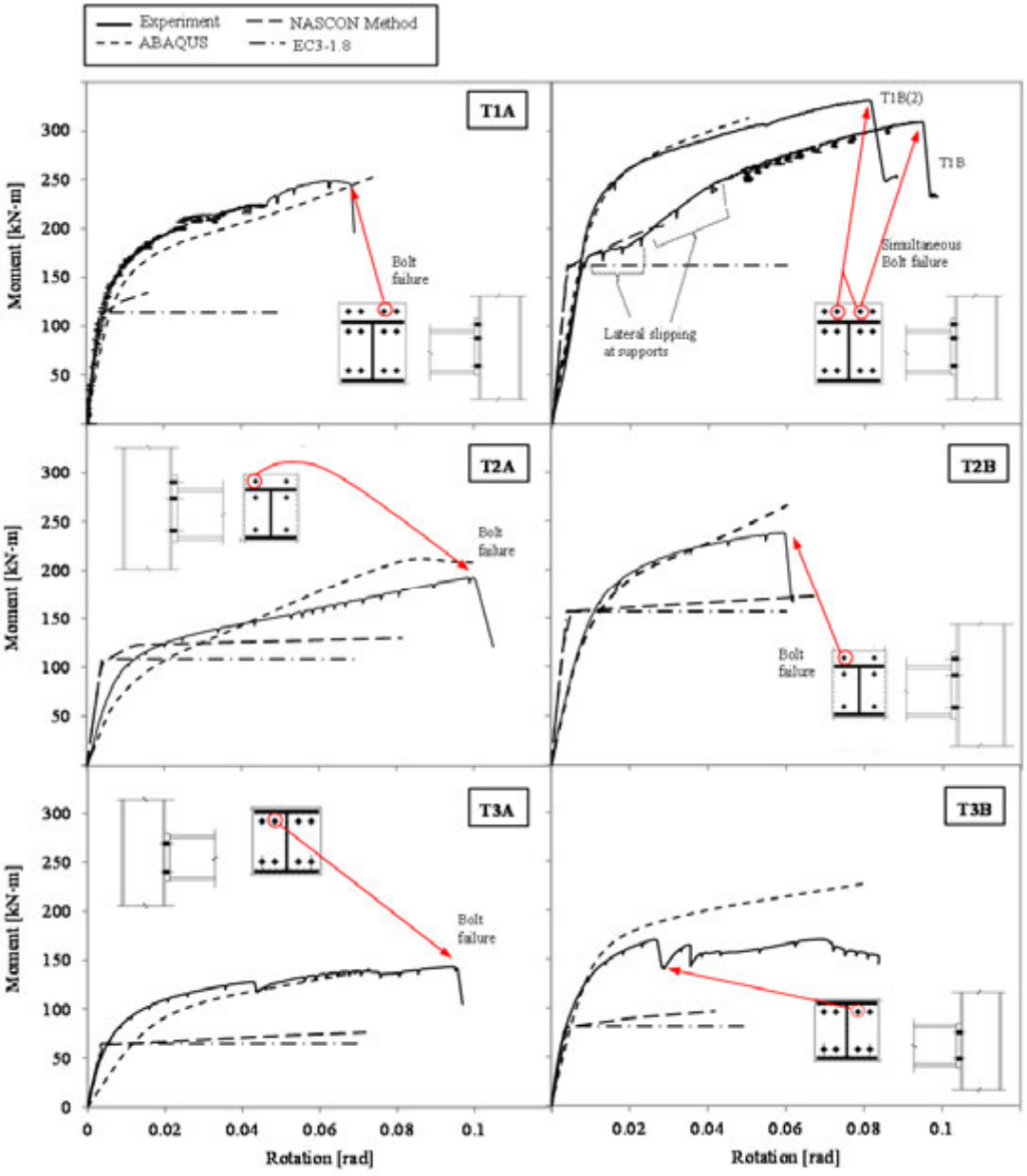

Figure 23. Comparison between experiment, ABAQUS simulation, and the NASCON method.

Table 4: Connection strength, stiffness, and rotation values for experimental testing, finite element analysis, and component methods.

	Specimen	No. of Bolts	Strength at 0.02rad [kN-m]	Initial Rotational Stiffness [kN-m]	Peak Rotation [rad]	Remark, classic Failure Limit State (Initial Yielding)	Ultimate Failure Limit State
Experimental Testing	T1A	12	193.5	26341	0.069	Column flange bending	Tensile bolt failure
	T2A	6	122.1	12346	0.105	Column flange bending	Tensile bolt failure
	T3A	8	109.8	14268	0.097	Column flange bending	Tensile bolt failure
	T1B	12	183.8	21153	0.098*	Column flange bending	Tensile bolt failure
	T1B(2)	12	262.4	22313	0.081	Column flange bending	Tensile bolt failure
	T2B	6	196.4	17577	0.062	Column flange bending	Tensile bolt failure
	T3B	8	161.3	27277	0.027**	Column flange bending	Bolt thread shear
Finite Element Analysis	T1A	12	179.3	19501	--***	Column flange bending	--***
	T2A	6	107.3	9140	--	Column flange bending	--
	T3A	8	96.9	5816	--	Column flange bending	--
	T1B	12	261.9	23802	--	Column flange bending	--
	T2B	6	190.2	17676	--	Column flange bending	--
	T3B	8	177.0	16367	--	Column flange bending	--
NASCON Method	T1A	12	133.6****	33625	--***	Column web compression	--***
	T2A	6	124.0	27824	--	Column flange bending	--
	T3A	8	66.6	16503	--	Column flange bending	--
	T1B	12	191.8	42140	--	Column flange bending	--
	T2B	6	160.8	39685	--	Column flange bending	--
	T3B	8	89.4	20290	--	Column flange bending	--
EC3 Component Method	T1A	12	114.0	33008	--***	Classified as semi-rigid	--***
	T2A	6	108.8	27420	--	Classified as semi-rigid	--
	T3A	8	64.7	18576	--	Classified as semi-rigid	--
	T1B	12	162.6	41835	--	Classified as semi-rigid	--
	T2B	6	156.5	38967	--	Classified as semi-rigid	--
	T3B	8	81.1	23824	--	Classified as semi-rigid	--

* Specimen experienced lateral slip during testing

** Reduction to 80% of ultimate capacity after 0.027rad, specimen regained strength and achieved 0.084rad

*** Not applicable

**** Failure predicted at 0.016 rad

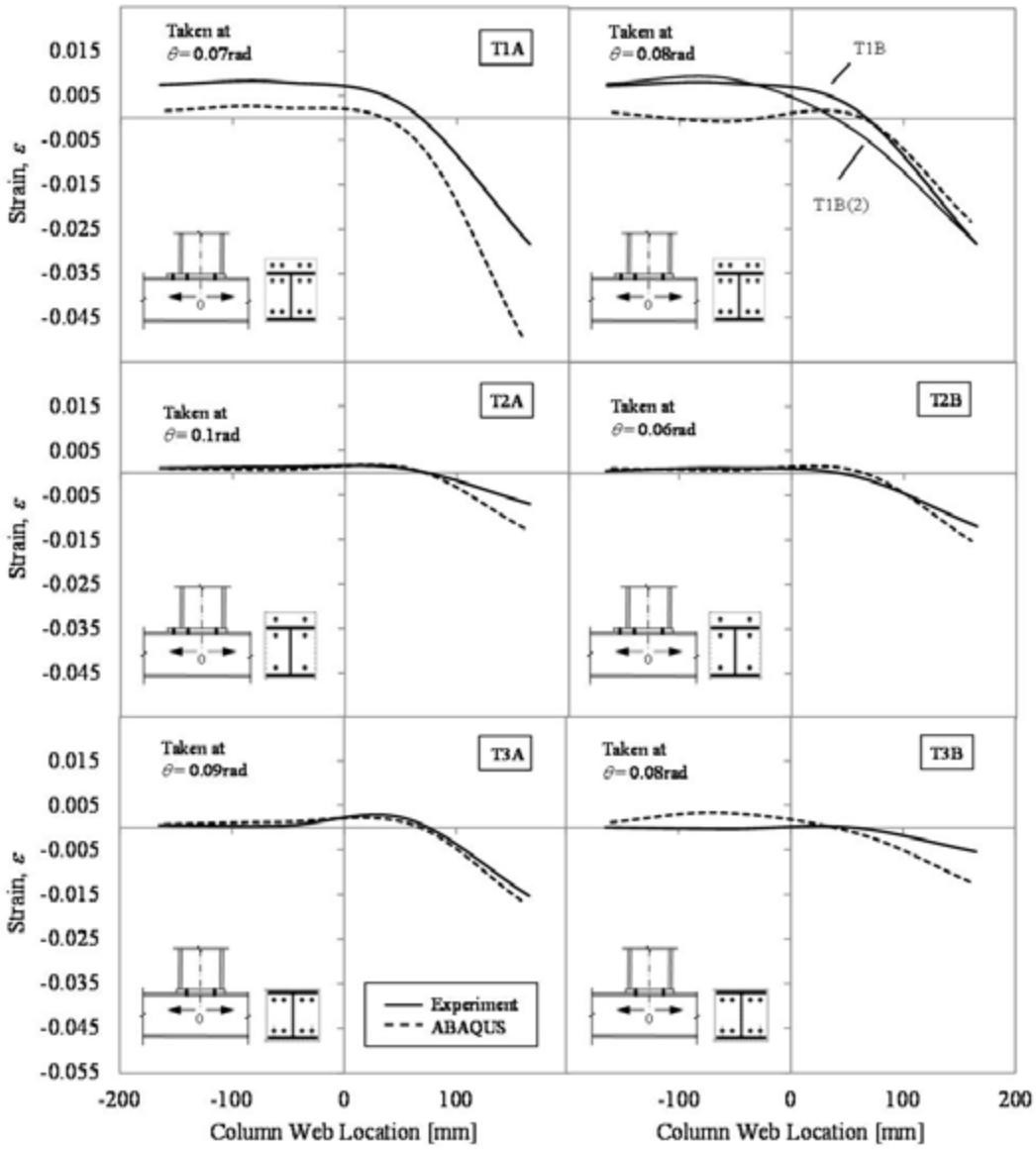

Figure 24. Comparison between strains from experiments and ABAQUS simulations.

6.2. Influence of Bolt Grouping on Bolt Demands

With bolt fracture ultimately limiting the rotation capacity of each test specimen, understanding the state of stress in each bolt can help identify potential performance issues between different bolt configurations. Figure 25 through Figure 27 show the individual column-flange bolt bearing stresses (obtained from finite element simulations) for configurations T1B, T2B, and T3B. While the bolt element was not explicitly modeled, equilibrium between the bolt and column flange allows insight into bolt stress distributions. As expected from the observed bolt fractures during testing, the closer the bolt is to the column web, the higher the stress in the bolt. In Figure 25 and Figure 27, having four bolts per row in the connection tensile region, stress concentrations occur in the inner bolts (those closest to the column web) on the inner bolt section, and reduce within the bolt section moving away from the column web (432 MPa to 373MPa in bolt 3 of configuration T1B, and 433 MPa to 375 MPa in bolt 3 of configuration T3B, see Figure 25 and Figure 27). These bolt stress concentrations and stress distributions are due to prying caused by

deformations between the column flange and beam endplate. Stress distributions in configuration T2B, having only two bolts per row, are more uniformly distributed across the bolt section similar to the exterior bolts in configurations T1B and T3B (compare Figure 26 with Figure 25 and Figure 27).

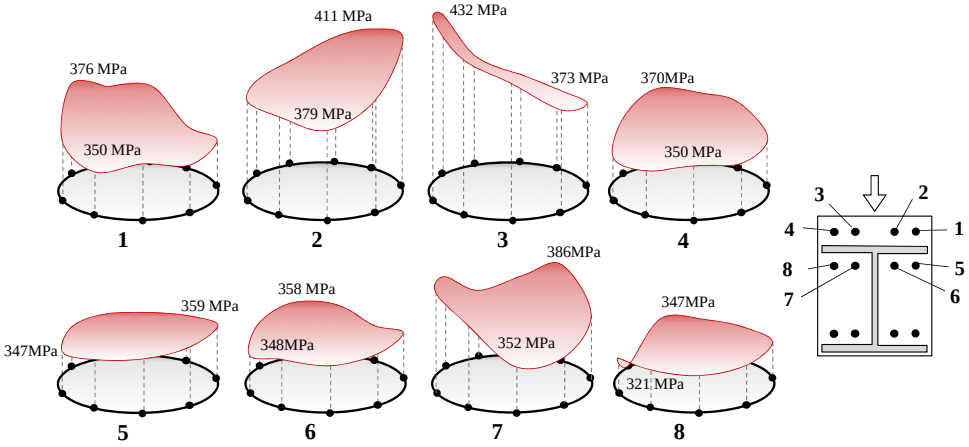

Figure 25. Bolt bearing stresses in column flange (connection T1B, values taken at ultimate moment from experimental testing).

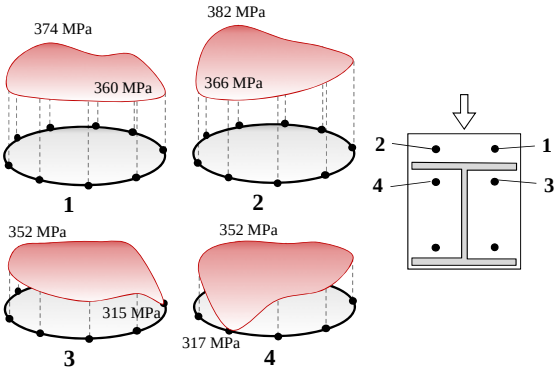

Figure 26. Bolt bearing stresses in column flange (connection T2B, values taken at rotation corresponding to ultimate moment from experimental testing).

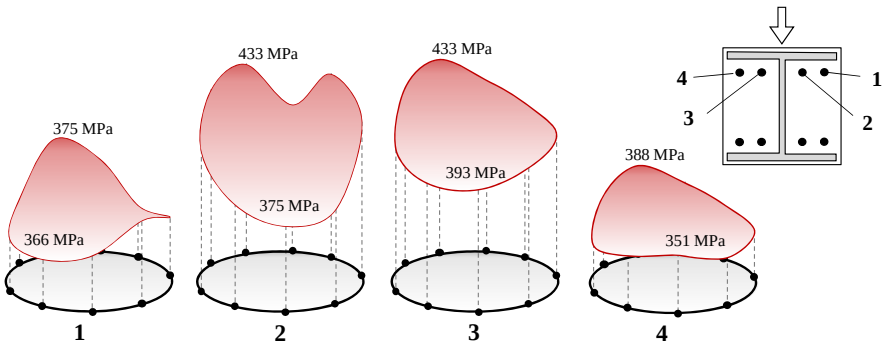

Figure 27. Bolt bearing stresses in column flange (connection T3B, values taken at rotation corresponding to ultimate moment from experimental testing).

6.3. Local Connection Stresses

Figure 28 shows the connection stresses for configurations T2A and T2B having identical bolt arrangements but different column section geometry (flange thickness of 14mm and 19mm, and web thickness of 8.5mm and 11mm for T2A and T2B respectively). Both configurations are shown at the same level of applied rotation (0.06rad) for direct comparison. With the increased column section dimensions in configuration T2B, the compressive and tensile stresses increased in the column web directly adjacent to the endplate. This is expected as the increased column-flange capacity allows for more load transfer into the column web. Stress distribution patterns between the two configurations are similar, and similar to the assumed compressive and tensile zones in the EC3-1.8 component method [2]. Figure 29 shows the detailed stress state in the connection tensile region of configuration T2A, including the column-flange bolt bearing stresses due to flange distortion.

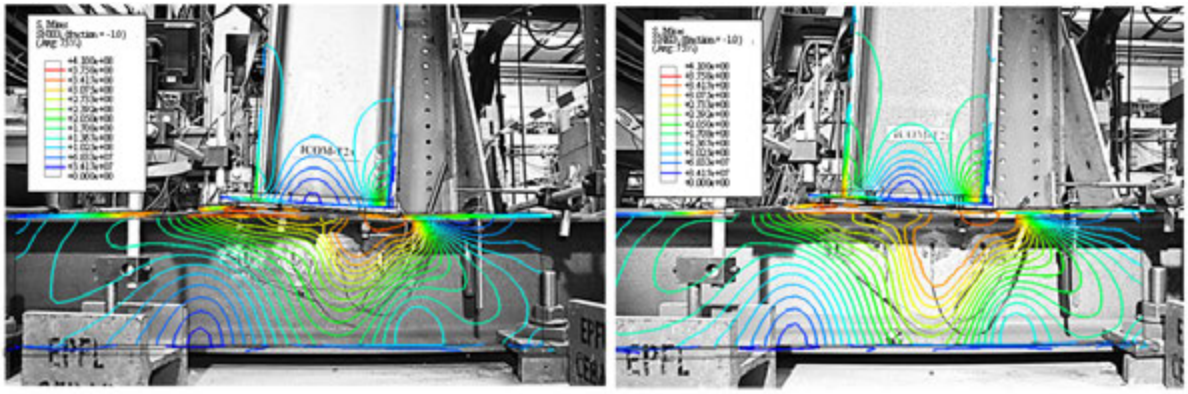

(a) (b)

Figure 28. Connection stress contours plotted over experimental deformations for a) T2A and b) T2B (all values are in N/m^2 and taken at 0.06rad of rotation for both connections).

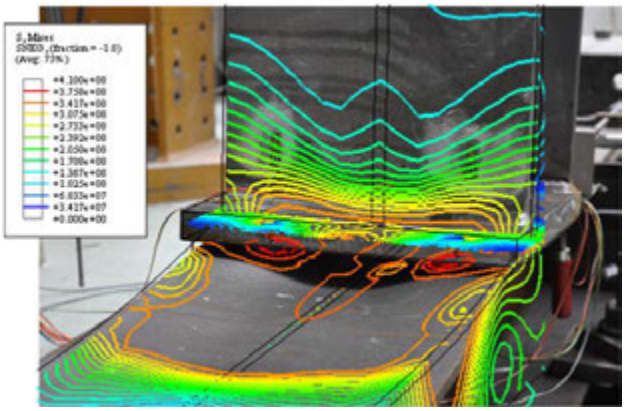

Figure 29. Connection stress contours plotted over experimental deformations for T2A (all values in N/m^2).

7. Summary and Conclusions

In this study, six beam-column configurations (seven experimental tests) having thick endplates and different bolt configurations, including configurations with multiple bolts per row, were tested to failure under static pushover loading. All configurations were fabricated without column web stiffeners in the column outside the bolted connection. The six

connection configurations represented two strength scenarios: 1) a weak-column strong-beam scenario (with H300A and H300B sections for the column and beam respectively), and 2) an equal-beam equal-column scenario (with H300B sections for both the column and beam). Additional analytical and numerical simulations validated from the experimental tests provided insight into local connection behavior. Global connection behavior from the experimental tests and local connection behavior from analytical simulations were compared with current code methods.

The following conclusions are based on the experimental testing and analytical and numerical simulation of the six beam-column connection configurations:

1) Deformations in the column section govern the failure of equal-column equal-beam or weak-column strong-beam connections when thick endplates are present (endplate greater than or equal to 1.5 times the flange thickness, and when column web stiffeners are not provided in the column). As bolt locations move toward the column web centerline, column flange distortions caused from the higher transverse stiffness of the column web, increase bolt prying forces. This has implications for configurations having multiple bolts per row, as limited space often requires positioning of bolts near the column web.

2) The use of multiple bolts per row increases connection moment capacity for both weak-column strong-beam and equal-column/beam scenarios (not containing column web stiffeners), but decreases rotation capacity (connection ductility) in weak-column strong-beam scenarios due to increased bolt prying forces and earlier bolt failure from column flange distortions (compare experimental result for specimen T1A and T2A in Figure 23). As the minimum rotation capacity for all tests (0.027rad) is far greater than the theoretical rotation required to obtain the P-P state for beams of reasonable length (see again Figure 22), this reduction in rotation capacity has no implication for creation of the Table C9 values.

3) As expected, connection rigidity increases with the use of multiple bolts per row and extended endplates.

4) As per an experimental/supply error, GR 4.6 washers were used in place of required GR 10.9 HV washers for each bolt in the beam-column tests. An exploratory T-Stub test confirms however, that the use of GR 4.6 washers rather than GR 10.9 HV washers has negligible effect on bolt pre-stress and bolt prying demands; global experimental test results are therefore expected to be similar had GR 10.9 HV washers been used during testing.

5) The two-dimensional connection representation with the NASCON method (based on EC3-1.8 component method) consistently under-predicted connection strength at the reference 0.02rad rotation, but correctly identified the flange bending initial limit-state. The EC3-1.8 component method values are always on the safe side by at least 11%, thus this method can be conservatively used to make the Table C9 values for cases having similar geometry to those tested herein (applicable to beam-column assemblies without column web stiffeners).

6) Finite element simulation with shell elements and nonlinear springs is a reasonably accurate method for determining global and local response of connections having thick endplates and multiple bolts per row. While such a method is too time consuming for generation of all Table C9 values, future experimental validation of

specific cases (where accurate determination of connection post-yield behavior is required) could be replaced by such advanced finite element simulations.

8. Future Work

While the connection configurations having four bolts per row and no column web stiffeners resulted in increased connection moment capacity, it is unclear whether this increase is a result of additional bolts or simply a closer spacing of the inner bolts to the column web. To investigate the specific bolt contributions in such configurations, further T-stub tests should be carried out with instrumented bolts (one T-stub having four bolts, and one having only two bolts but with the same inner bolt spacing as with the four bolt configuration). Figure 30 shows possible bolt configurations for the further T-stub testing.

In addition to T-stub testing, the accuracy of the finite element methods presented within the report should be verified with beam-column connections having column web stiffeners. The modeling methods could then be used to investigate stiffener effects on the configurations tested within this report. As future work, such techniques could be verified using existing experimental tests performed by others.

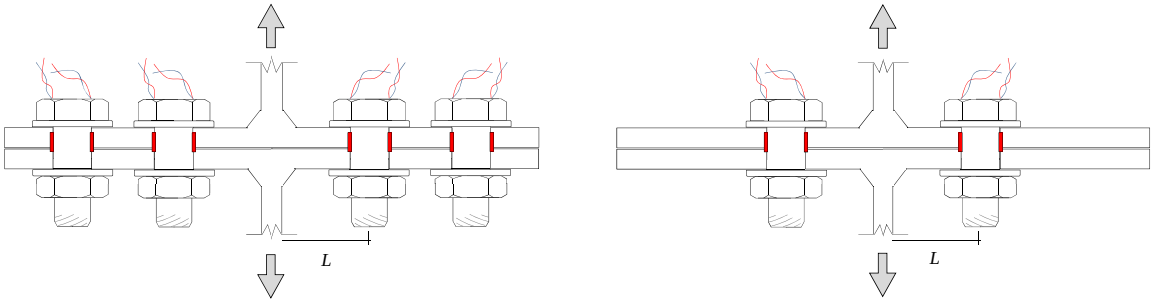

Figure 30. Four and two bolt T-stub configurations having the same inner bolt spacing.

9. References

[1] Jones, S. W., Kirby, P.A. and Nethercort, D.A. (1983). "The analysis of frames with semi-rigid connections - A state-of-the-art report." *J. Constructional Steel Research.* **3**(2): 2-13.

[2] Eurocode_3 (1993). "Design of steel structures part 1-8: design of joints." *European Standard EN 1993-1-8.* European Committee for Standardization, Brussels, Belgium.

[3] Zoetenmeijer, P. (1983). "Summary of the research on bolted beam-to-column connections (period 1978-1983)." *Report No. 6-85-M.* Steven Laboratory, Delft.

[4] Zoetenmeijer, P. (1983). "Proposal for standarisation of extended end plate connection based on test results." *Report No. 6-83-23.* Steven Laboratory, Delft.

[5] Aggarwal, A. K. a. C., R.C. (1986). "Moment-rotation characteristics of bolted beam-column connections." *J. Constructional Steel Research.* **6**(1986): 303-318.

[6] Aggarwal, A. K. a. C., R.C. (1987). "Strength criteria for bolted beam-column connections." *J. Constructional Steel Research.* **7**(1987): 213-227.

[7] Davison, J. B., Kirby, P.A., and Nethercot, D.A. (1987). "Rotational stiffness characteristics of steel beam-to-column connections." *J. Constructional Steel Research.* **8**(1987): 17-54.

[8] Popov, E. P. a. T., S.M. (2002). "Bolted large seismic steel beam-to-column connections Part 1: experimental study." *Eng. Structures.* **24**(2002): 1523-1534.

[9] Kukreti, A. R. a. Z., F.-F. (2006). "Eight-bolt endplate connection and its influence on frame behavior." *Eng. Structures.* **28**(2006): 1483-1493.

[10] Bahaari, M. R. a. S., A.N. (2000). "Behavior of eight-bolt large capacity endplate connections." *Computers and Structures.* **77**(2000): 315-325.

[11] Shi, Y., Shi, G. and Want, Y. (2007). "Experimental and theoretical analysis of the moment-rotation behavior of stiffened extended end-plate connections." *J. Constructional Steel Research.* **63**(2007): 1279-1293.

[12] Shi, G., Shi, Y., Wang, Y. and Bradford, M.A. (2008). "Numerical simulation of steel pretensioned bolted end-plate connections of different types and details." *Eng. Structures.* **30**(2008): 2677-2686.

[13] Abidelah, A., Bouchair, A., and Kerdal, D.E. (2012). "Experimental and analytical behavior of bolted end-plate connections with or withour stiffeners." *J. Constructional Steel Research.* **76**(2012): 13-27.

[14] Demonceau, J.-F., Jaspart, J.-P., Weynand, K., Oerder, R., and Muller, C. (2011). "Connections with four bolts per horizontal row." *Proc. Eurosteel.* Budapest, Hungary.

[15] SZS (1997). "Tables pour la construction metallique." *C5/97.* Centre Suisse de la Construction Metallique, Zurich, Switzerland.

[16] SZS (2006). "Tables de dimensionnement " *C4/06.* Centre Suisse de la Construction Metallique, Zurich, Switzerland.

[17] HKS (2006). "ABAQUS Standard Users manual, Version 6.4." Hibbitt, Karlsson, and Sorensen, Inc.

[18] Gervásio, H., Simões da Silva, L., Borges, L., "Reliability assessment of the post-limit stiffness and ductility of steel joints", *J. of Constructional Steel Research*, **60** (2004): 635-648 (issues 3-5).

[19] Borges, L., "Evaluation of the Rotation Capacity of Steel Joints", MSc Dissertation, University of Coimbra, Coimbra, Portugal, 2003.

ÉCOLE POLYTECHNIQUE
FÉDÉRALE DE LAUSANNE

FACULTE ENVIRONNEMENT NATUREL, ARCHITECTURAL ET CONSTRUIT (ENAC)
INSTITUT D'INGENIERIE STRUCTURALE (IIC)
LABORATOIRE DE LA CONSTRUCTION METALLIQUE (ICOM)

Rapport EPFL N° 181194/1

Bolted Steel Connections having Multiple Bolts per Row, T-Stub Testing in view of use with the component method

Gary S. Prinz, Ph.D., P.E.
Prof. Alain Nussbaumer, Ph.D.

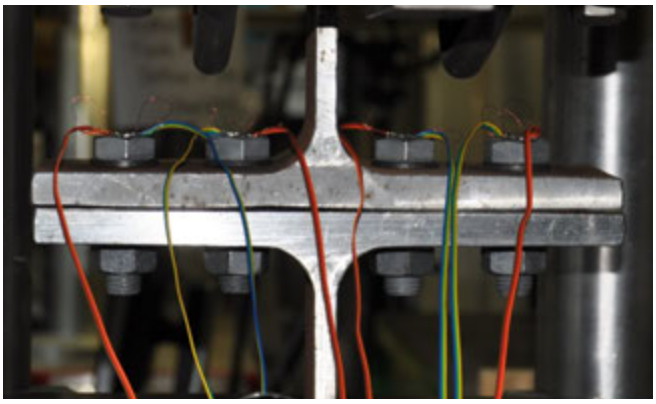

August, 2013

Introduction

Understanding the strength and rigidity of connection regions is necessary for the efficient design of steel building systems. The required strength of beams and columns depends directly on considerations made for the connection rigidity. To estimate the true strength and rigidity characteristics of bolted beam-column connections, the EuroCode has adopted the component method, which considers individual connection components (bolts, flanges, webs, endplates, etc.) and their interactions. One of the component is called T-stub.

Thus, in addition to the work carried in [1], the behavior of T-stubs was of interest to us. The additional tests carried out are presented herein.

T-Stub Testing

To explore the influence of washer strength on bolt demands and to further explore (beyond the testing in [1]) bolt participation in configurations having multiple bolts per row, three T-stub connections are tested. The T-stubs represent beam-column connection demands for situations where column web stiffeners are not included. The first T-stub connection (specimen TS1) explores the influence of washer strength on bolt prying and bolt pre-stress using GR10.9 HV bolts and both GR4.6 and GR10.9 washers. The next two T-stub connections (specimens TS2 and TS3) consider four bolt-per-row and two bolt-per-row configurations, having the same inner-bolt spacing (spacing between the T-stub web and inner bolt). Figure 1(a) shows the setup for specimen TS1 including T-stub geometry and bolt locations; Figure 2 shows the setup for specimens TS2 and TS3.

The T-stub connections are fabricated from an HE300B section cut in half at the web centerline, and tested in a universal testing machine with a 1000kN capacity. Similar to the beam-column experiments, all bolts are pre-tightened to 480N-m as per [2] using a pre-set torque wrench. Each bolt is instrumented with two unidirectional strain gauges positioned 180 degrees apart and fixed near the bolt surface (see Figure 1(b)). Attaching gauges on opposite sides of the bolt surface allows for determination of prying strains during expected deformations of the T-stub.

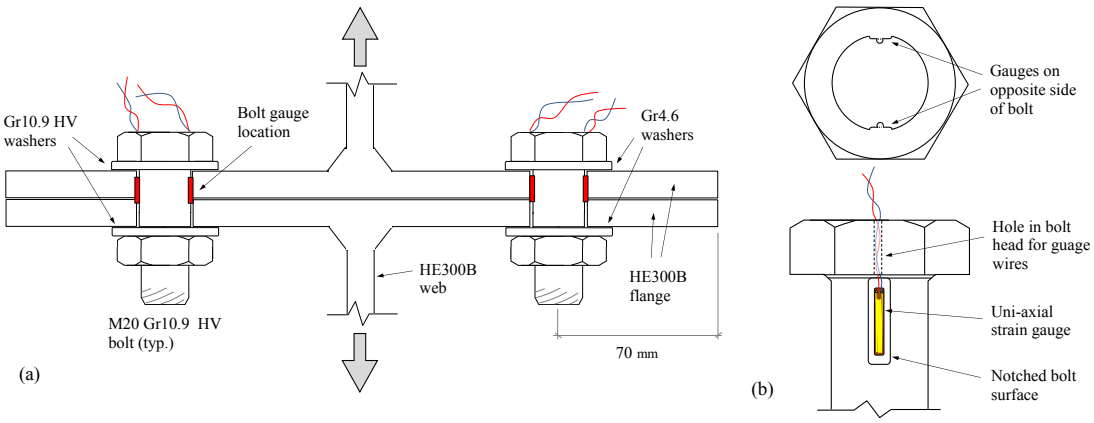

Figure 1. (a) Specimen TS1 geometry and bolt locations (b) bolt instrumentation (all T-stub specimens)

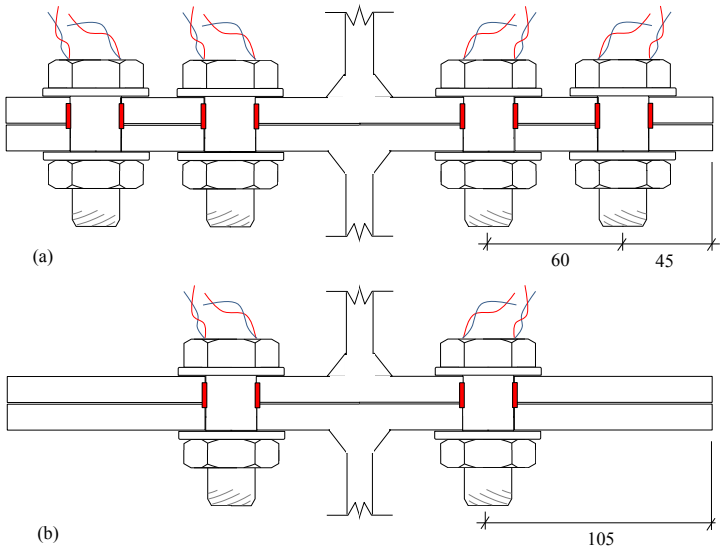

Figure 2. (a) Specimen TS2 having four bolts-per-row and (b) specimen TS3 having two bolts-per-row.

Effect of GR4.6 Washers on Bolt Load and Pre-Stress

The use of GR 4.6 washers, rather than GR 10.9 HV washers, has negligible effect on the applied bolt pre-stress. Figure 3 shows the measured axial pre-stress between the bolts having GR 4.6 and GR 10.9 HV washers, with less than 15MPa difference after the applied torque. This indicates similar friction resistance for both washer strengths, and suggests accurate application of bolt pre-stress in the beam-column tests of [1].

Measured prying strains between the two bolts were similar, but slightly larger for the GR 10.9 HV bolt. During testing of the T-stub connection, failure of the GR 10.9 HV bolt governed the connection capacity. Figure 4 shows the distribution of strains in each bolt at the peak applied load, and Figure 5 shows the evolution of bolt surface strains during loading. From Figure 4, similar strain distributions are observed between the two bolts, with a 26% higher maximum tensile strain value for the bolt having a GR 10.9 HV washer. In Figure 5, this significant bolt prying occurs near an applied load of 300kN; however, as evident in Figure 5, bolt bending is also induced from the applied pre-tensioning.

Similar pre-stress values and prying strains between the two bolts suggests that the GR 4.6 washers had a negligible effect on the experimental values obtained for the beam-column specimens.

Calculations using the EC3-1.8 T-stub capacity equations suggest flange yielding as the governing T-stub failure mode. From the EC3-1.8 calculations, the flange yielding capacity (mode 1 failure) is calculated as 169kN whereas capacities for mode 2 (flange-yielding with bolt fracture, including prying) and mode 3 (bolt tensile fracture) are 228kN and 352kN respectively. Comparing calculated capacities with the T-stub response in Figure 5, the predicted limit state of flange yielding is overly conservative; however, the EC3-1.8 method appears to predict the mode 2 failure limit (bolt fracture with flange yielding) with reasonably accuracy.

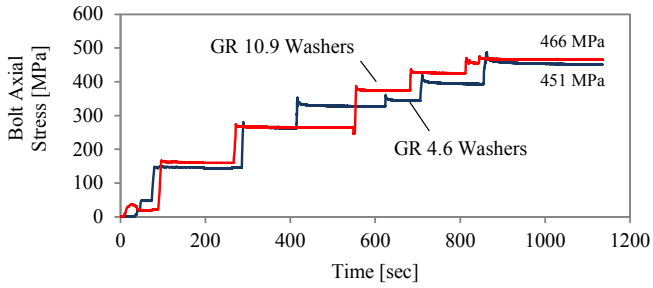

Figure 3. Measured bolt axial pre-stress.

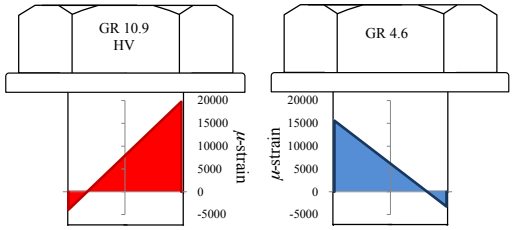

Figure 4. Peak measured surface strains

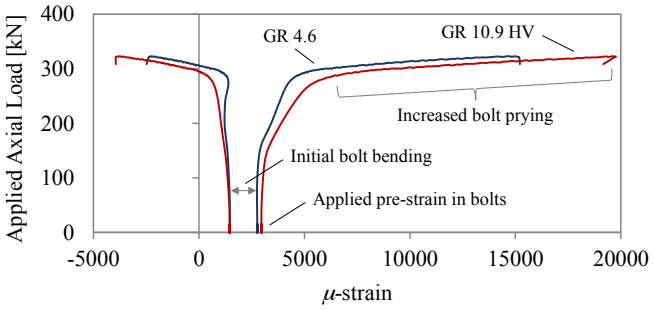

Figure 5. Evolution of bolt surface strains during loading.

Bolt Participation in Configurations having Multiple Bolts per Row

The outer bolt in the four-bolt-per-row configuration does not contribute to the T-stub resistance until fracture of the inner bolt occurs. Figure 6 presents the axial and prying strain demands within the bolts of specimens TS2 and TS3, with the inner bolt taking the entire applied load. In Figure 6, both the axial and prying strains in the outer bolt of specimen TS2 actually decrease during increased loading. Strain demands on the inner bolt are essentially the same between the two configurations. Bolt thread shear was the governing failure mode for both tests, and a similar failure load of near 500kN was reached.

Bolts having closer spacing to the T-stub web experience lower prying strains and higher strength. Comparing bolt prying demands and connection strength between all three T-stub tests (see Figure 6(b)), the critical bolt prying strain for specimen TS1 was reached after 323kN while the critical prying strain for the bolts of TS2 and TS3 were reached after 514kN and 483kN respectively. With similar strength and bolt demands between the TS2 and TS3 T-stub configurations, along with increased prying in specimen TS1 having a larger inner-bolt spacing, the increased strength of the four-bolt-per-row beam-column specimens in [1] can be directly attributed to bolt spacing relative to the column web.

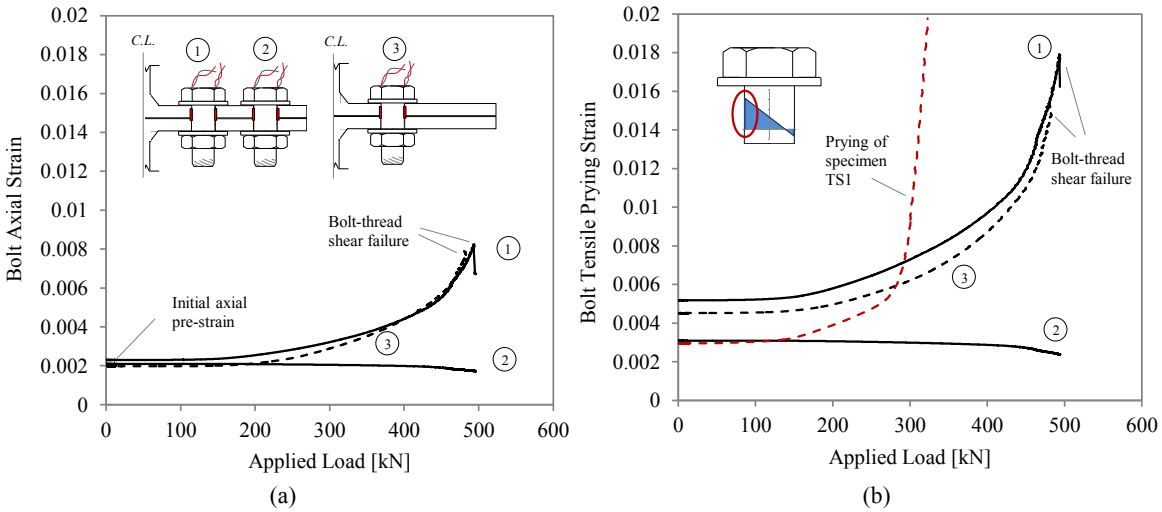

Figure 6. Bolt participation versus T-stub load for configurations having four and two bolts-per-row: (a) bolt axial strain comparison and (b) bolt prying strain comparison.

1. References

[1] Prinz, G. S., Nussbaumer, A., and Khadka, S. (2013). "Experimental testing and simulation of bolted beam-column connections having thick extended endplates and multiple bolts per row." *Report EPFL No. 181194.* Mandat No. IC 707.

[2] SZS (1997). "Tables pour la construction metallique." *C5/97.* Centre Suisse de la Construction Metallique, Zurich, Switzerland.